ELSEVIER

Geotextiles and Geomembranes 16 (1998) 311–331

Geotextiles and Geomembranes

Limit analysis in stability calculations of reinforced soil structures

Radoslaw L. Michalowski*

Department of Civil Engineering, The Johns Hopkins University Baltimore, MD 21218, USA

Received 23 April 1998; received in revised form 18 July 1998

Abstract

Stability analyses of reinforced soil structures are traditionally based on limit equilibrium calculations. Results from such analyses are sometimes ambiguous because of different assumptions made in addition to the limit state. It is shown in this paper that these ambiguities can be removed if the kinematic approach of limit analysis is used, in which a rigorous bound to the required strength of reinforcement is sought. The required strength of reinforcement is the strength needed to maintain stability of the structure. Since limit analysis leads to a rigorous bound on the reinforcement strength, limit loads, or a safety factor, the geometry of the failure mechanisms considered can be optimized, so that the best bound is obtained (a solution closest to the exact solution). A dual formulation of kinematic limit analysis is possible in terms of limit force equilibrium, but the former is preferable since the kinematics of collapse mechanisms appeals to engineering intuition more than the distribution of forces does. © 1998 Elsevier Science Ltd.

Keywords: Soil reinforcement; Geosynthetics; Stability; Limit analysis

1. Introduction

This paper reviews an existing method of limit analysis in the context of design of reinforced soil structures. The application of the method is also illustrated with an example of a slope. However, there are some new elements: in particular, the controversial issue of inclination of the reinforcement force at a failure surface is resolved with a new conclusion. Also, results from a new experimental study on collapse of a reinforced subgrade are shown. These results are presented here as an example of an

* Fax: 410 516-7473; e-mail: rlm@jhu.edu

0266–1144/98/$ – see front matter
PII: S0266–1144(98)00015–6

effort to identify failure mechanisms of reinforced soil that can be used later in the kinematic approach of limit analysis.

In the last 20 years or so there have been numerous efforts made to set guidelines for calculations of stability of reinforced slopes, walls, and embankments. Such calculations need to be able to indicate what the safety margin of a given structure is, or how much reinforcement is necessary to construct a new structure. As a result, a number of different suggestions have been proposed in the literature. An example is a multitude of results based on a two-block failure mechanism for stability calculations of reinforced slopes. One might expect that once the same mechanism is selected, the required reinforcement strength calculated or the factor of safety should be identical, but the literature shows otherwise. It seems useful then to introduce a method of analysis that would remove ambiguities found in traditional techniques, and, perhaps, to make it possible to assess the existing solutions.

This paper is written to illustrate and to clarify some of the aspects of limit analysis of reinforced soil structures, and not to criticize existing methods. Many of the existing approximate analyses for stability calculations of reinforced soil have served well in design, and this paper is written to indicate how these calculations can be improved. Stability considerations are only one aspect of what is a much broader design process, which, in addition, must address such issues as constructability, drainage, possible damage to geosynthetics prior to installation, etc. (see Koerner, 1998; Holtz et al., 1997).

Limit analysis is an approach to stability calculations based on two theorems that make it possible to find rigorous bounds (upper and lower) to unknown quantities, such as the critical height of a reinforced slope, limit force on a footing (bearing capacity), etc. Alternatively, for given structures and given loads an estimate of material parameters necessary to maintain stability can be found. Thus, the technique can be used, for instance, for calculations of the amount of reinforcement necessary to maintain stability.

This technique was first suggested for reinforced soil analysis in the late 1980s, with two approaches: (1) the continuum approach, where the soil and reinforcement are first homogenized, and the anisotropic continuum is considered, and (2) the structural approach, where reinforcement is considered as separate structural members. The continuum-based approach can be found, for instance, in papers by de Buhan et al. (1989), and Sawicki and Leśniewska (1989), while the structural approach was used by Anthoine (1989), and de Buhan and Salençon (1993). The latter is often called a mixed approach, since the reinforcement is considered as structural members and the soil is considered as a continuum. A comparison of the two techniques was presented by Michalowski and Zhao (1995). Only limit analysis as applied to the structural approach is discussed in this paper.

A dual formulation of the kinematic limit analysis in terms of equilibrium of limit forces is possible (Salençon, 1990). Application of the limit force equilibrium approach can be found in papers of Leshchinsky and Boedecker (1989) and Jewell (1990). These have been successfully used in practice. A review of techniques used for stability analyses of reinforced soil structures (including force equilibrium), in the context of seismic loads, was presented recently by Bathurst and Alfaro (1996). The author chose

the technique based on the kinematic approach, since kinematics of the failure mechanism appeals to engineering intuition more than the distribution of forces does. The method of analysis is illustrated in this paper in examples of slopes, but it is applicable to reinforced walls, embankments, reinforced subgrades, and unpaved roads.

2. Limit analysis

Limit analysis was presented in terms of the theorems by Drucker et al. (1952), but the concept was known earlier (Gvozdev, 1938; Hill, 1948). The material involved in the analysis obeys a convex yield condition, such as the Mohr–Coulomb criterion

$$f(\sigma_{ij}) = (\sigma_x + \sigma_y)\sin\varphi - \sqrt{(\sigma_x - \sigma_y)^2 + 4\tau_{xy}^2} + 2c\cos\varphi = 0, \tag{1}$$

where c and φ are the cohesion and internal friction angle of the soil, respectively, and its plastic deformation is governed by the normality (or associative) flow rule

$$\dot{\varepsilon}_{ij}^{pl} = \dot{\lambda}\frac{\partial f(\sigma_{ij})}{\partial \sigma_{ij}}, \qquad \begin{array}{ll} \dot{\lambda} \geqslant 0 & \text{if } f = 0, \\ \dot{\lambda} = 0 & \text{if } f < 0, \end{array} \tag{2}$$

where $\dot{\lambda}$ is a nonnegative scalar multiplier, $f(\sigma_{ij})$ is the yield criterion, and $\dot{\varepsilon}_{ij}^{pl}$ and σ_{ij} are the plastic strain rate and the stress tensor, respectively.

The upper bound theorem is based on construction of admissible collapse mechanisms (or velocity fields), and it states that *if a kinematically admissible mechanism is found, then the limit load calculated by equating the rate of work of external forces to the rate of internal energy dissipation is not smaller than the true limit load.* It is useful to write this theorem in a mathematical form

$$\int_V \dot{D}(\dot{\varepsilon}_{ij})dV \geqslant \int_{S_v} T_i \mathrm{v}_i dS_v + \int_{S_t} T_i \mathrm{v}_i dS_t + \int_V \gamma_i \mathrm{v}_i dV. \tag{3}$$

The left-hand side of inequality (3) represents the rate of work dissipation during an incipient failure of a structure, and the right-hand side includes the work rates of all the external forces. T_i is the stress vector on boundaries S_v and S_t. Vector T_i is unknown (limit load) on S_v, and it is known on S_t (for instance, surcharge pressure). v_i is the velocity vector in the kinematically admissible mechanism, γ_i is the specific weight vector, and V is the volume of the mechanism. Thus, the mathematical form of the theorem in Eq. (3) states that the rate of energy dissipation is not less than the rate of work of external forces in any kinematically admissible failure mechanism. Hence, the inequality in Eq. (3) can be used to calculate the upper bound to the force on boundary S_v, if all the other terms in Eq. (3) are known. Notice that the total force on boundary S_v can be calculated only if velocity v_i on this boundary is constant. On the other hand, if all the loads acting on a structure are given, the material parameters necessary to maintain the limit state can be evaluated from Eq. (3). A lower bound to

one such parameter can be calculated from Eq. (3). For reinforced soil structures this parameter may be the strength of the reinforcement. Alternatively, if the geometry of the structure is given, and all loads and material parameters are known, the safety factor can be calculated from Eq. (3). An application of Eq. (3) to a simple mechanism of a slope failure will be illustrated later in this paper.

The static approach of limit analysis (leading to lower bounds on limit loads, or upper bounds on the material properties necessary to maintain limit equilibrium) is based on constructing admissible stress fields (see, for instance, Davis, 1968). The static theorem is seldom used in geotechnical engineering since admissible stress fields are difficult to construct.

3. Admissibility of collapse mechanisms

A crucial element in the application of the theorem in Eq. (3) is the construction of an admissible failure mechanism. The flow rule in Eq. (2) leads to a well-defined dilatancy in the deforming soil, and it is illustrated in Fig. 1(a). The rate of internal work (or dissipation) in a unit volume of a deforming soil can be calculated as (see, for instance, Davis 1968)

$$\dot{d} = (\dot{\varepsilon}_1 - \dot{\varepsilon}_3)\, c \cos\varphi, \tag{4}$$

where $\dot{\varepsilon}_1$ and $\dot{\varepsilon}_3$ are the major and minor principal strain rates. Thus, integrating Eq. (4) over the deforming regions in a failure mechanism yields the left-hand side in Eq. (3). Very useful mechanisms are those where rigid blocks are separated by velocity discontinuities. The work is then dissipated only on interfaces between the blocks. The associative flow rule (Eq. (2)) requires that the velocity jump vector be inclined to these discontinuities at angle φ (Fig. 1(b)), and the work dissipation rate per unit area of

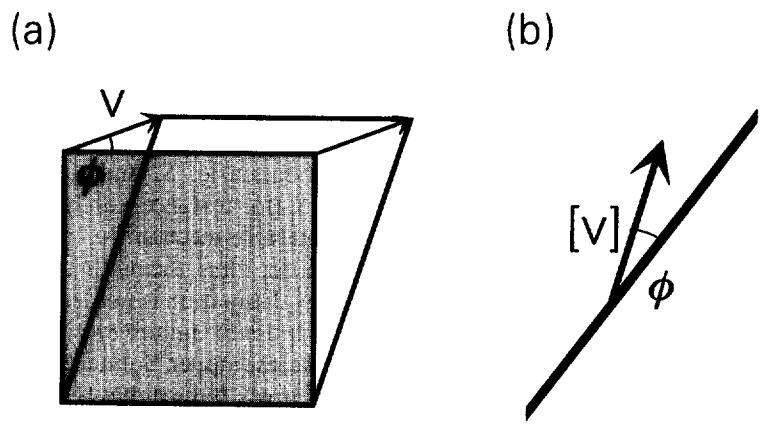

Fig. 1. Example of admissible plastic deformation of granular material: (a) simple shear, and (b) velocity discontinuity.

such discontinuity surface can be found from

$$\dot{d} = c\,[\mathrm{v}]\cos\varphi \tag{5}$$

where [v] is the magnitude of the velocity discontinuity vector.

An important part of constructing failure mechanisms is a hodograph. An example of an admissible collapse mechanism for a slope is shown in Fig. 2(a). The kinematic boundary condition here is v_0 – the vertical component of the velocity of the first (top) block. The three blocks move with velocities v_1, v_2, and v_3, respectively. Since velocity v_1 must be inclined to discontinuity AB at angle φ, velocity $[v]_{12}$ is inclined at φ to discontinuity BO, etc., the hodograph can be constructed with uniquely determined velocities, Fig. 2(b). These velocities can be calculated numerically from the geometrical relations in the hodograph. The mechanism in Fig. 2(a) belongs to the class of translational mechanisms, since all blocks translate without rotation.

A kinematically admissible rotational mechanism is shown in Fig. 2(c). The entire region *ABC* rotates as a rigid block with velocity $\dot{\omega}$ about point *O*. Thus, the velocity at any point in region *ABC* can be calculated as $r\dot{\omega}$, where *r* is the radius from the rotation center to the point considered. Since kinematical admissibility requires that velocities are inclined at angle φ to failure surface *BC*, line *BC* must be a log-spiral. Only if $\varphi = 0$ can failure surface *BC* be a circular arc, otherwise, a circular arc is inconsistent with the rigid rotation velocity field.

Examples of kinematically inadmissible mechanisms used in the limit equilibrium method are shown in Fig. 3. In the two-block mechanism the force between the blocks is inclined to the interface normal at angle $\delta < \varphi$. Such a mechanism is inadmissible since the velocity discontinuity cannot occur along *BD* unless the Mohr–Coulomb yield condition is reached ($\delta = \varphi$). To indicate quantitative consequences of assuming $\delta < \varphi$, calculations were performed for a slope with $\beta = 60^\circ$ and $\varphi = 35^\circ$ (granular

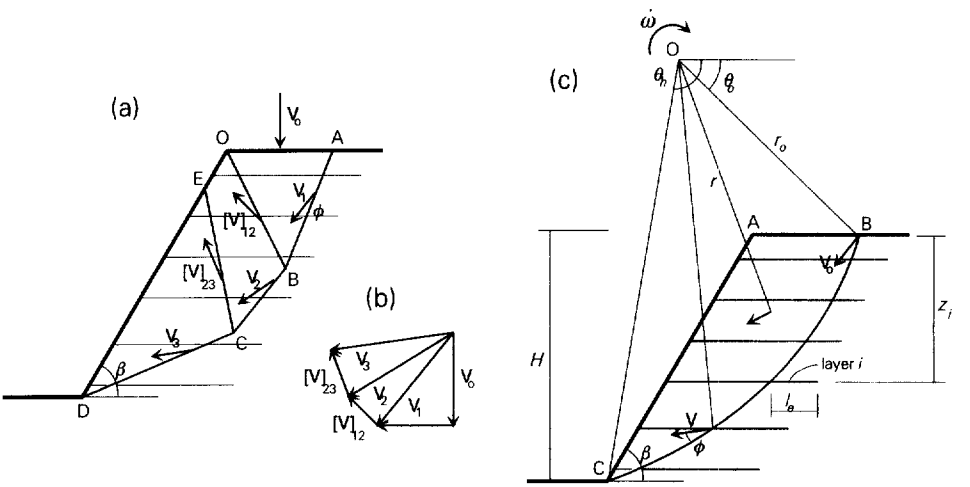

Fig. 2. Kinematically admissible mechanisms of slope failure: (a) translational mechanism, (b) hodograph, and (c) rotational collapse mechanism.

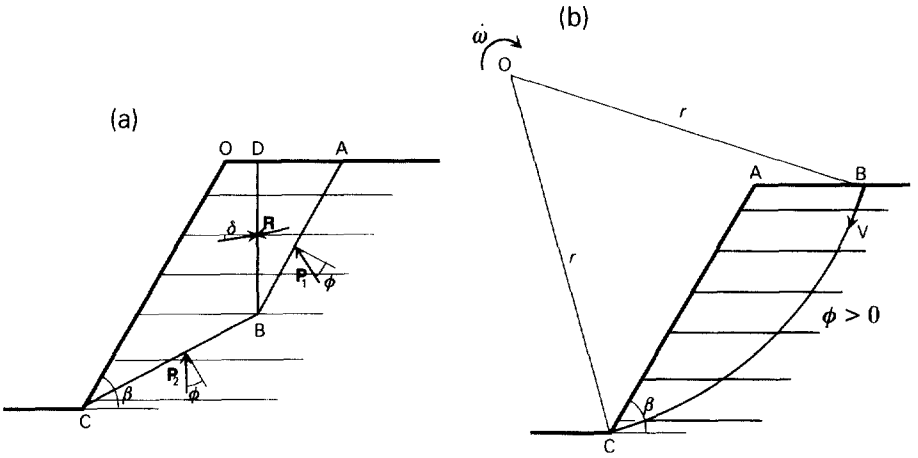

Fig. 3. Inadmissible mechanisms: (a) yield condition not satisfied on surface *BD*, and (b) rigid-rotation mechanism with circular arc failure surface in frictional soil.

soil), for a three-block mechanism (Fig. 2(a)) and a two-block mechanism (Fig. 3(a)) with angle $\delta = 0$ on all 'internal' failure surfaces. The reinforcement is uniformly distributed, and its strength is characterized by an average magnitude k_t

$$k_t = \frac{nT_t}{H}, \tag{6}$$

where n is the number of reinforcement layers, T_t is the tensile strength of a single reinforcement layer (per unit width), and H is the height of the slope. The inclination of all failure surfaces was taken such that the calculated magnitude of k_t was the maximum (since this approach leads to a lower bound on k_t). The calculated dimensionless average strength $k_t/\gamma H$ (γ being the unit weight of the soil) is $k_t/\gamma H = 0.0752$ and $k_t/\gamma H = 0.0663$ for the three-block and two-block mechanisms, respectively. These are approximate solutions which can be proved to be neither upper nor lower estimates of the true solution. The term 'true solution' here relates to the exact solution to the limit state problem, which is subject to constraints imposed by the boundary conditions and the soil model used (Mohr–Coulomb failure criterion, associativity of the deformation process). The best rigorous lower bound to $k_t/\gamma H$ (the largest of those calculated based on all known admissible mechanisms) is the one based on Fig. 2(c): $k_t/\gamma H = 0.0570$. Assuming $\delta = 0$ leads to overestimation of the best solution to the necessary reinforcement strength (32% and 16% for the three- and two-block mechanism, respectively). This does not come as a surprise, since assuming $\delta < \varphi$ is equivalent to reducing the actual strength of the soil.

An example of another kinematically inadmissible mechanism includes rigid rotation in a frictional soil with a circular arc failure surface (Fig. 3(b)). It is evident that the

velocity discontinuity vector is tangent to the failure surface, thus it violates the kinematic admissibility for dilative material (Fig. 1(b)).

It should be emphasized that both limit analysis and limit equilibrium are approximate techniques. Rigorous limit analysis, however, yields a strict bound to the true solution, and, if a number of realistic mechanisms are considered and optimized, then a solution reasonably close to the true solution can be expected (this has been shown for some geotechnical problems by achieving a small difference between the rigorous upper and lower bounds, Michalowski and Shi, 1993). The solution to the necessary reinforcement strength based on the mechanism in Fig. 2(c) happens to be the best strict lower bound to the true solution, but it has not been proved to be the true (exact) solution.

4. Failure of reinforcement

Application of the kinematic theorem to reinforced soils requires that, in addition to the work dissipation in soil, internal work due to plastic failure (or pullout) of reinforcement be calculated and included in the term on the left-hand side of Eq. (3). A rigorous limit analysis solution for a problem with reinforcement will be obtained only if the mechanism of collapse considered is admissible, i.e., the deformation of the soil is compatible with the deformation of the reinforcement. Examples of such deformation are shown in Fig 4. The schematic in Fig. 4(a) relates to collapse of a flexible reinforcement (such as a geotextile or geogrid) when intersected by a failure surface (velocity discontinuity). The failure surface is considered here as a finite-thickness layer with a high velocity gradient. This reinforcement contributes to stability only through its tensile strength. If the reinforcement fails after reaching its tensile limit force T_t, then the work dissipation rate during incipient failure can be calculated (Michalowski and Zhao, 1995) by integrating the product of the limit force and the elongation strain rate within section AB of the reinforcement (Fig. 4(a))

$$\dot{D} = \int_0^{t/\sin\eta} T_t \langle \dot{\varepsilon}_l \rangle \, \mathrm{d}x = T_t [\mathrm{v}] \cos(\eta - \varphi), \tag{7}$$

where T_t is the limit tensile force (taken as positive) in the reinforcement sheet per unit width, and η is the angle of inclination of the reinforcement layer to the failure surface, Fig. 4(a). The strain rate in the reinforcement is taken as positive in tension $\langle \dot{\varepsilon}_l \rangle = [\mathrm{v}] \cos(\eta - \varphi) \sin\eta/t$, and $\langle \dot{\varepsilon}_l \rangle = 0$ when $\eta - \varphi > \pi/2$ (the ability of reinforcement to resist compression is disregarded due to possible buckling and kinking). The work dissipation rate can thus be calculated directly as the dot product of the limit force and the velocity jump vector. This type of reinforcement failure is often referred to as tensile rupture.

In rigid-block failure mechanisms, the work dissipation in reinforcement takes place only within the shear bands between the blocks, since the strain rate within the rigid blocks is zero. However, elasto–plastic deformation of reinforced soil takes place prior to the instant of failure.

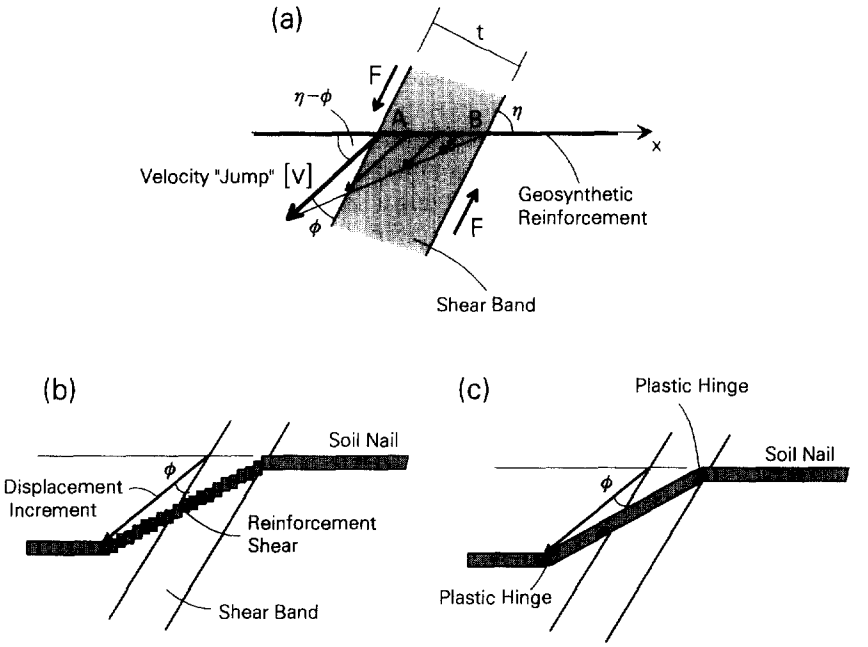

Fig. 4. Collapse of reinforcement: (a) tensile failure of a flexible reinforcement, (b) shear failure of a soil nail, and (c) plastic hinge formation.

Possible failure mechanisms of reinforcement with shear and flexural strength, such as soil nails, are shown in Figs. 4(b) and (c). In the first one the reinforcement shears, and the second one is associated with the formation of two plastic hinges (see de Buhan and Salençon, 1993). This paper will concentrate only on the reinforcement with tensile strength.

The controversial issue of reinforcement force inclination was discussed by Wright and Duncan (1991) in the context of the limit equilibrium method as applied to reinforced slopes. Engineering intuition is often used to indicate that, after a small deformation increment, the reinforcement is no longer horizontal at a failure surface (Fig. 5(a)), and the direction of the limit force in the reinforcement taken into the analysis is not well-defined. This ambiguity is easily removed by using the kinematic approach of limit analysis: the most accurate solution (the best bound) is one where the safety factor is minimized, or the required strength of reinforcement is maximized. It follows then that the horizontal reinforcement leads to the best limit analysis solution. This argument is disputable, however, since it is not clear whether or not an arbitrary inclination of the reinforcement force is admissible.

A more detailed argument is made below that the reinforcement force direction should be taken as horizontal (direction of the reinforcement original placement). First, the argument is made based on the limit equilibrium approach.

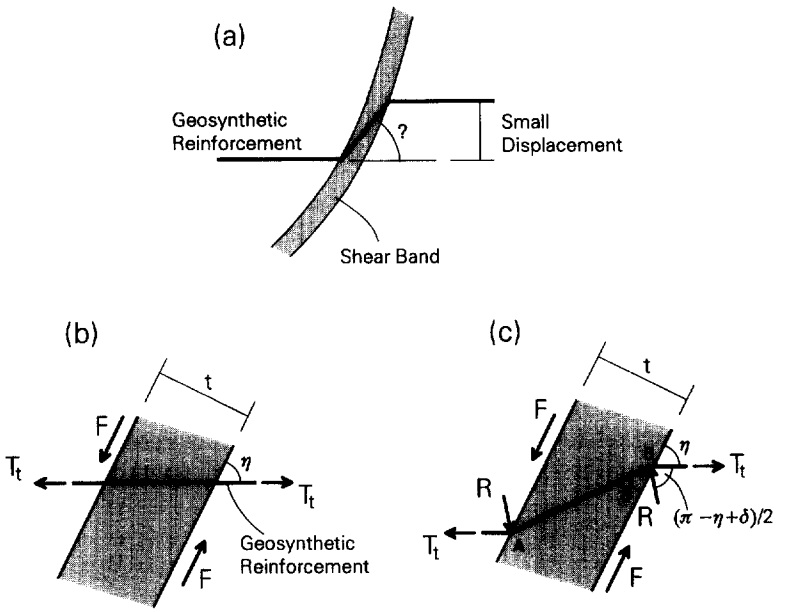

Fig. 5. Schematic for analysis of force inclination at failure surface: (a) small displacement of geosynthetic at failure zone, (b) horizontal reinforcement, and (c) forces acting on displaced reinforcement.

Consider a portion of the failure layer as in Fig. 5(b). The resistance to shear along that segment consists of the soil shear strength and the contribution of the reinforcement. It will be shown that the reinforcement contribution to the shear resistance, F, is independent of whether the reinforcing layer is horizontal (Fig. 5(b)) or its configuration is altered due to a small shear along the failure surface (Fig. 5(c)).

If the force in the reinforcement reaches its limit, T_t, the contribution of the horizontal reinforcement to the shear resistance at the failure surface can be calculated directly as

$$F = T_t \sin\eta \tan\varphi + T_t \cos\eta, \tag{8}$$

where angle η is shown in Fig. 5(b), and T_t is the tensile strength of the reinforcement per unit width. Physically, some deformation is needed to mobilize the limit force in reinforcement. However, Eq. (8) is consistent with the rigid-perfectly plastic material (used in limit equilibrium method), which requires only infinitesimal deformation before full strength is mobilized. The same result can be obtained using the kinematic approach of limit analysis. The energy dissipation rate is given in Eq. (7), and the work rate of the limit shear force F is

$$\dot{W} = F\,[\mathrm{v}]\cos\varphi \tag{9}$$

(see Fig. 4(a) for [v]). Now, equating the rate of dissipation in Eq. (7) and the work rate in Eq. (9), and solving for F, the result is identical to that in Eq. (8).

The limit equilibrium method is based on the premise that the soil is in limit equilibrium, and the reinforcement is in limit equilibrium, but the two do not interact at the failure zone (Fig. 5(b)). Consequently, the resistance to shear of the two components, soil and reinforcement, are directly additive. However, once the sliding increment has occurred prior to failure, the interaction of the reinforcement and the soil can no longer be ignored (Fig. 5(c)). Thus, if inclined limit force T_l (in the direction AB, Fig. 5(c)) is taken in the free body diagram in limit equilibrium calculations, reaction R must also be considered. The contribution of the reinforcement to the shear resistance along the failure surface now becomes

$$F = T_l \sin\delta \tan\varphi + T_l \cos\delta + R\cos\frac{\eta + \delta}{2}\tan\varphi - R\sin\frac{\eta + \delta}{2} \tag{10}$$

(see Fig. 5(c) for angle δ). The magnitude of reaction R is now calculated from the moment equilibrium of two force couples acting on the reinforcement, Fig. 5(c) (all other forces acting on the reinforcement within the shear band are self-equilibrated)

$$R = 2T_l \sin\frac{\eta - \delta}{2}. \tag{11}$$

Upon substitution of Eq. (11) into Eq. (10), Eq. (8) is recovered again, so the two analyses yield the same result. Eq. (10) is more indicative of the true mobilization process than is Eq. (8). The analysis shows that the resistance to shear is unique, but taking the horizontal direction of the reinforcement force into the analysis is more straightforward. Hence, the direction of the reinforcement limit force at the failure surface considered in the analysis should be taken parallel to the original direction of placement (typically horizontal). If it is taken as inclined, then an additional soil-reinforcement interaction force needs to be taken into account, which is typically ignored in limit equilibrium analyses. However, deformed reinforcement has an effect on the stability analysis if it fails by pull-out. This is because the pull-out force of curved reinforcement is increased due to the belt friction effect. Displacements of reinforcement at a failure surface were studied by Gourc et al. (1986) in the context of a 'displacement method'. This paper does not make use of the results by Gourc et al. (1986).

The argument from the limit analysis standpoint is similar to that given above. If the mechanism includes the entire shear band, then the reinforcement force is horizontal, and the energy dissipation rate can be calculated as in Eq. (7). If the mechanism cuts through the inclined portion of the reinforcement (Fig. 5(c)), then the work dissipation rate (left-hand side of Eq. (3)) increases due to inclination of the limit reinforcement force, but the reaction force R now becomes an external force, and its work needs to be included on the right-hand side of Eq. (3). In either case, the result is the same.

In order to indicate quantitative consequences of including inclination of the reinforcement force in stability analysis, but ignoring the soil-reinforcement interaction force, calculations were performed to evaluate the amount of reinforcement necessary to maintain limit equilibrium of slopes. The soil is granular (no cohesion),

and the reinforcement strength is characterized by its average magnitude k_t (see Eq. (6)). The results are given in Fig. 6 in dimensionless form $k_t/\gamma H$ (γ being the unit weight of the soil), for a range of slope inclination angles (β) from 40° to 90°, and for internal friction angle (φ) of 20°, 30°, and 40°. The mechanism in Fig. 2(c) was used in limit analysis calculations, uniform distribution of reinforcement was considered, and the reinforcement force inclination was assumed to be collinear with the velocity jump vector along failure surface BC. The solid lines in Fig. 6 represent the rigorous lower bounds to the strength of reinforcement necessary to maintain stability, and the dashed lines indicate reinforcement calculated with inclined reinforcement forces and disregarding the soil-reinforcement interaction. It is clear that ignoring the soil-structure interaction forces leads to underestimation of the necessary reinforcement strength. This underestimation is small for soils with a large internal friction angle. For instance, it is 12% for a vertical slope and $\varphi = 40°$, and it becomes negligible for slopes with an inclination angle less than 60°. However, this underestimation becomes substantial when the soil internal friction angle is low (26% for a vertical slope and $\varphi = 20°$). Although the realistic internal friction angle for granular soils does not drop below about 32°, lower values are likely to be used in design once the safety factor is applied. Hence, assuming inclined reinforcement forces in the analysis may have an adverse effect on the safety of designed slopes.

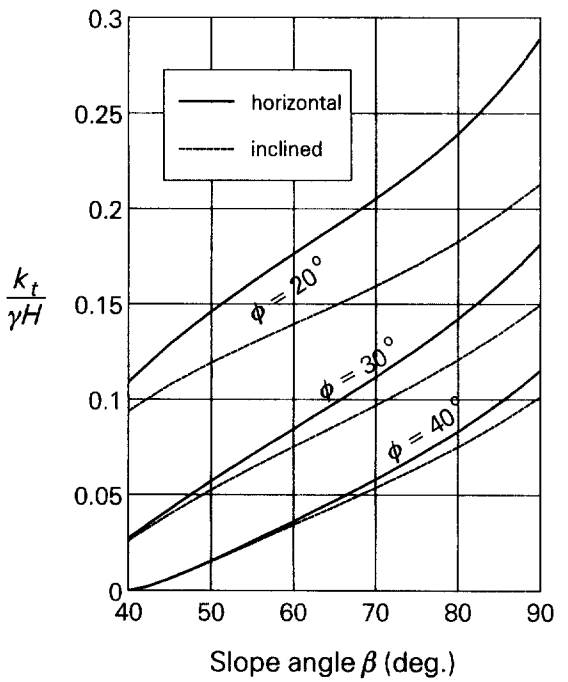

Fig. 6. Comparison of the reinforcement strength for slopes assuming horizontal and inclined reinforcement forces.

The contribution of the reinforcement to stability of a structure is included in limit analysis through the dissipative term on the left-hand-side of Eq. (3). The energy dissipation needs to be integrated over all of the reinforcement layers, and for each layer it needs to be summed over all of the intersections with rupture surfaces. For instance, the dissipation rate in the second layer (from the top) in Fig. 2(a) is the sum of the dissipation rates at rupture surfaces *AB*, *OB* and *EC*. Similarly, in the limit equilibrium method, the interaction force between the blocks must include the limit force in the reinforcement. However, this is typically neglected, and the reinforcement forces are only considered on the outer failure surfaces (for instance, *AB* and *BC* in Fig. 3(a)). Neglecting the contribution of the reinforcement at some of the rupture surfaces leads to kinematical inadmissibility, since the mechanism (for instance that in Fig. 3(a)) cannot occur unless the reinforcement along all of the rupture surfaces (including *BD* in Fig. 3(a)) is in the limit state. Consequently, the solution from the limit equilibrium method, where the contribution of reinforcement is ignored at some of the rupture surfaces, can be proved to be neither an upper nor a lower estimate of the true solution.

The second mode of failure of tensile reinforcement is pull-out from the soil. The work dissipation rate can be calculated for pull-out in a way similar to that for tensile rupture, but with the tensile strength replaced by the pull-out force

$$\dot{D} = T_p[\mathrm{v}]\cos(\eta - \varphi). \tag{12}$$

Assuming the coefficient of friction between the reinforcement and the soil is μ, the pull-out force can be calculated as

$$T_p = 2l_e \gamma z^* \mu, \tag{13}$$

where γz^* is the overburden pressure, and l_e is the effective length of reinforcement (see Fig. 2(c)). Coefficient μ is often given as a fraction of the tangent of the internal friction angle ($\mu = f_b \tan\varphi$). The pull-out force, T_p, should be taken in calculations of the work dissipation rate whenever it is smaller that the tensile limit force, T_t.

It should be noticed that the expression in Eq. (13) is approximate, since the stress on the reinforcement is taken as being approximately equal to the overburden pressure. While this is a reasonable (and generally accepted) method for calculating the pull-out force, the estimate of the limit forces or reinforcement strength calculated from Eq. (3) becomes an approximate solution, and not a strict bound.

Patterns of failure of other reinforced soil structures may not be as intuitively obvious as those for slopes. Therefore, experimental studies may be useful for identifying the collapse patterns for limit analysis calculations. Results from a study of reinforced subgrade collapse are shown in Figs. 7 and 8 (Shi, 1996; Michalowski and Shi, 1997). A small strip footing (width $B = 32$ mm) was loaded over a medium sand bed reinforced with strips of geotextiles at a depth of $0.4B$. The image of the sand under the footing (plane strain) was recorded in small intervals with a digital camera. The process of identifying the displacement field involved a computer technique, referred to in computer science terminology as a correlation-based motion detection technique, an alternative to stereophotogrammetry.

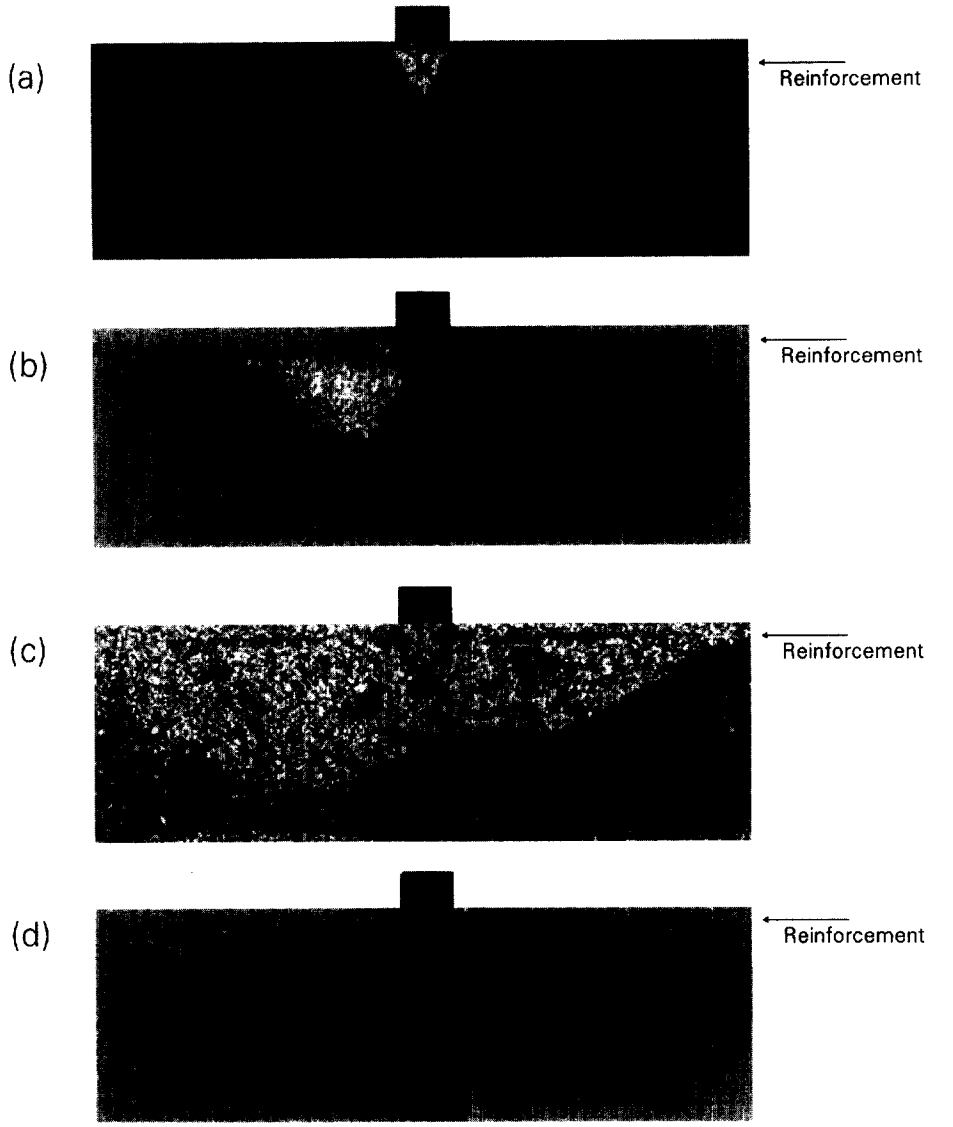

Fig. 7. Near-failure stage of loading of reinforced subgrade: (a) vertical displacement increments, (b) horizontal displacement increments, (c) shear strain increments, and (d) volumetric strain increments.

The pairs of record files (converted into sets of pixels with varying light intensity, or gray scale) were processed, where a square *template window* with a fixed number of pixels on one image was matched by a *candidate match window* on the second image. When a successful match was found, the displacement vector was identified by subtracting the coordinates of the corresponding windows. This process was performed directly on the computer files, without printing the actual images.

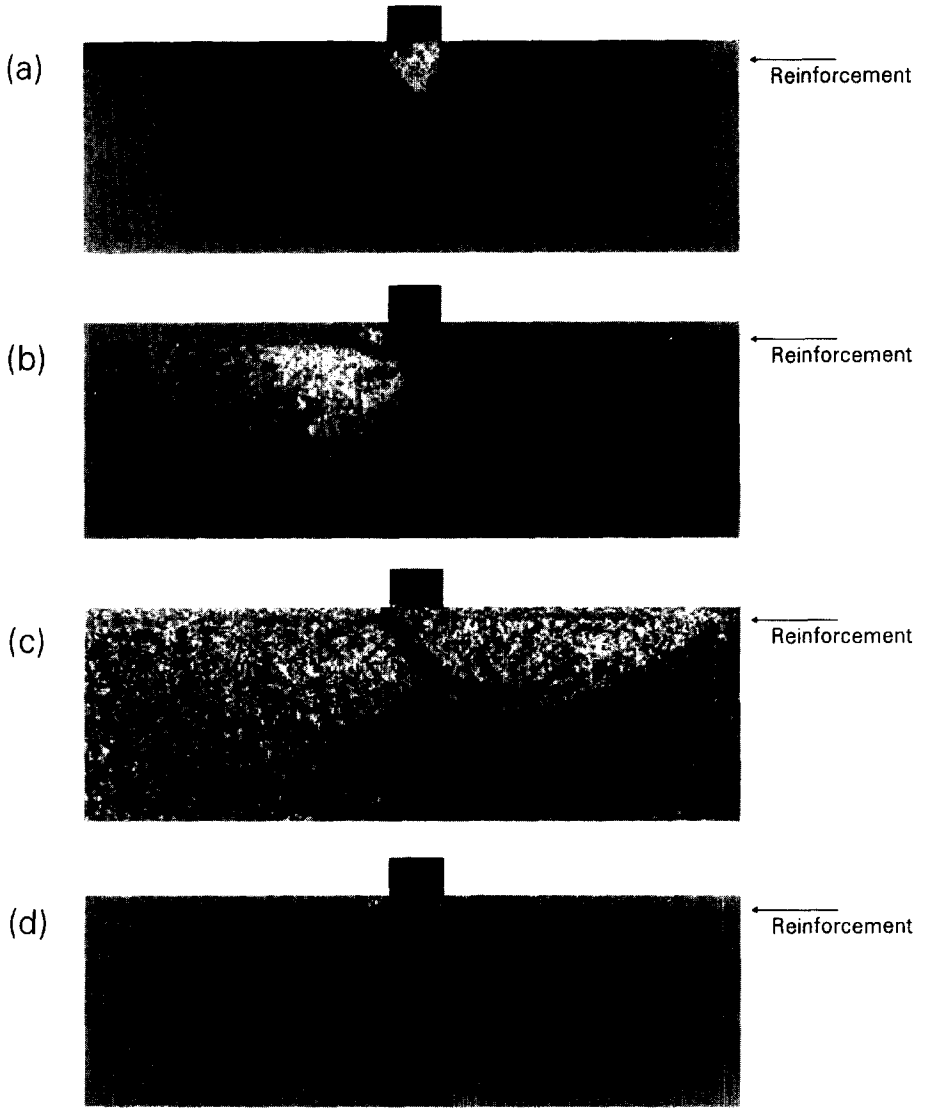

Fig. 8. Post-failure stage of loading of reinforced subgrade: (a) vertical displacement increments, (b) horizontal displacement increments, (c) shear strain increments, and (d) volumetric strain increments.

The pattern of vertical and horizontal components of displacement increments, at the stage where the footing was close to failure, are shown in Figs. 7(a) and (b). The color code used to depict the intensity of displacement increments did not convert well to the gray scale; however, these images are shown here only to indicate the failure patterns qualitatively. The maximum shear strain increments, calculated based on the displacement increments, are shown in Fig. 7(c).

As expected, the soil underneath the footing moves vertically down, and the soil on both sides of the footing moves upward. The distribution of horizontal displacement increments has an interesting feature: the sand moves approximately symmetrically sideways, but the soil above the reinforcement moves horizontally only in the close neighborhood of the footing. The reinforcement prevents horizontal displacements of this layer (but not vertical displacements). Consequently, a clear shear band is formed along the reinforcement (Fig. 7(c)). The pattern of shear strain increments is not quite symmetric, with a larger extent of distributed shear on the left-hand-side, and with a more distinct shear band propagating to the right. In the post-failure stage (Fig. 8) the collapse becomes clearly nonsymmetric. The reinforcement is being pulled out from the soil mass on the left-hand side of the footing. The shear band along the reinforcement is associated with a clear dilation effect (Fig. 8(d)). The reinforcement still prevents the horizontal displacements in the sand above, therefore the dilatancy causes an upward movement of the sand layer above the reinforcement (see the left-hand side of Fig. 8(a)).

The pattern of failure described is characteristic of strong reinforcement relative to the stress level in the soil. For large footings, a different failure pattern can occur where the reinforcement fails by rupture.

The above is an example of an effort to identify the mechanisms of failure which can be used in the kinematic approach of limit analysis. Only the qualitative interpretation of the small-scale tests is useful.

5. Optimization of collapse mechanisms

Once a type of failure mechanism is selected for use in kinematic limit analysis, its geometry need not be specified *a priori*. Instead, the specific geometrical parameters should be found from an optimization procedure where the best bound is sought. Examples of admissible mechanisms for a slope collapse are shown in Fig. 9. The first one is the simplest possible mechanism where the collapse occurs along surface BC. The specific geometry of the failure mechanism is described here by only one parameter: angle θ. Let the height of the slope be given, the soil be cohesionless ($c = 0$), and the amount of reinforcement necessary to avoid collapse be the unknown (nT_t, n being the number of reinforcement layers). Let the reinforcement be long enough so that collapse occurs only through tensile failure, not pull-out. The work dissipation rate in the soil is zero when $c = 0$ (see Eq. (5)), and the energy is dissipated during collapse only in the reinforcement (Eq. (7)). According to Eq. (3), equating the work dissipation rate in the reinforcement to the rate of work of the weight of block ABC leads to the lower bound on the amount of reinforcement necessary to avoid slope collapse. Notice that the slope is not loaded on its surface, so the only nonzero term on the right-hand side of Eq. (3) is the self-weight term. To illustrate the application of Eq. (3), we write it here after substitution of the respective terms for the mechanism in Fig. 9(a)

$$nT_t \mathrm{v}\cos(\theta - \varphi) = S_{ABC}\gamma \mathrm{v}\sin(\theta - \varphi) = \frac{\gamma H^2}{2}(\cot\theta - \cot\beta)\mathrm{v}\sin(\theta - \varphi), \qquad (14)$$

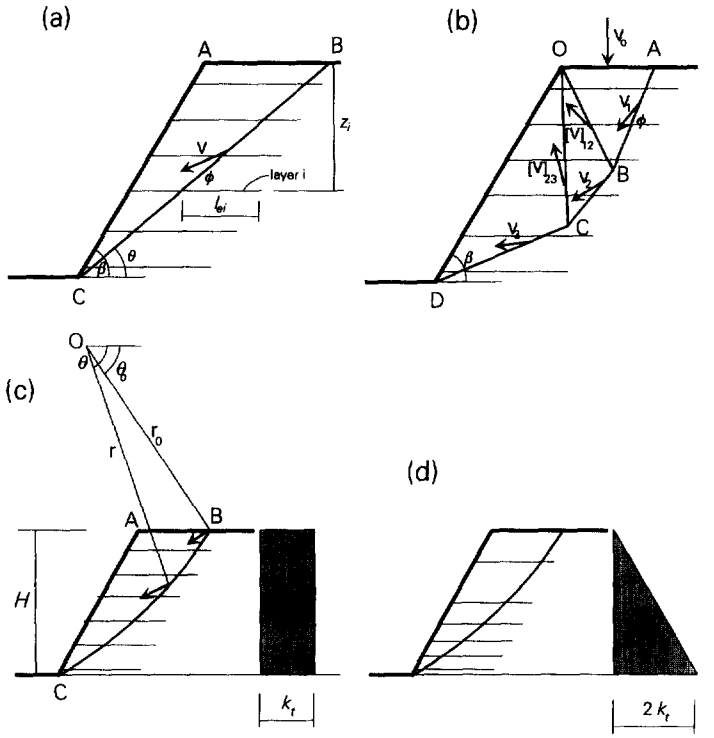

Fig. 9. Admissible slope failure mechanisms: (a) single-block mechanism, (b) multi-block pattern, (c) rotational collapse – uniform reinforcement, and (d) varied spacing of reinforcement.

where n is the number of reinforcement layers, v is the velocity of block ABC, and S_{ABC} is its area. Then the lower bound to the amount of reinforcement can be solved for

$$\frac{nT_t}{\gamma H^2} = \frac{k_t}{\gamma H} = \frac{1}{2}(\cot\theta - \cot\beta)\tan(\theta - \varphi), \tag{15}$$

where k_t is a convenient measure of the average reinforcement strength as introduced in Eq. (6). Now, since the formula in Eq. (15) yields the lower bound to $k_t/\gamma H$, the maximum of $k_t/\gamma H$ is the best bound, and it can be found from the condition

$$\frac{\mathrm{d}\left(\dfrac{k_t}{\gamma H}\right)}{\mathrm{d}\theta} = 0. \tag{16}$$

This solution is not likely to yield a good lower bound (close to the true reinforcement strength necessary for slope stability) because the mechanism considered is very restrictive, with only one variable (θ). The mechanism in Fig. 9(b) is more 'flexible' (with 5 variable angles), and it is likely to yield a much better bound. The velocities in

this mechanism are related through the geometrical relations in the hodograph (which can be constructed in a way similar to that in Fig. 2(b)). Both of these collapse patterns are in the class of translational mechanisms.

A rotational mechanism is shown in Fig. 9(c). Block ABC rotates about point O, and the reinforcement yields along failure surface BC. Such a mechanism is kinematically admissible only if surface BC is log-spiral $r = r_0 \exp\{(\theta - \theta_0)\tan\varphi\}$, since only then will the velocity jump vector along BC be inclined to it at angle φ. The lower bound to $k_t/\gamma H$ can be found in the same way as for the simple one-block mechanism, though the specific expressions for the work rates are more elaborate (see Michalowski, 1997). Calculations of the best lower bound to the exact value of $k_t/\gamma H$ for a 60^0 slope (and $\varphi = 35^0$), using the three mechanisms in Fig. 9(a–c), yield $k_t/\gamma H = 0.0378$, $k_t/\gamma H = 0.0433$, and $k_t/\gamma H = 0.0570$, respectively ($k_t/\gamma H = 0.0529$ for the mechanism in Fig. 2(a) where the rupture surfaces are not forced to originate from point O). Hence the rotational mechanism yields the best solution, since it gives the highest lower bound.

Once the dimensionless strength of the reinforcement, $k_t/\gamma H$, necessary to maintain stability is determined, one can use the relation $k_t = nT_t/H$ to calculate the necessary number of layers if reinforcement strength is given (or vice-versa).

This section can be concluded with the following remark: it is crucial in the stability analysis that the mechanisms considered are kinematically admissible, and that they are optimized to obtain the best bound possible. Assuming, for instance, that rupture surface BD in Fig. 3(a) is vertical is a significant constraint on the mechanism, which will lead to a poor estimate of the true solution. For instance, for a slope with $\beta = 60°$ and $\varphi = 35°$ (and $\delta = \varphi$), the mechanism in Fig. 3(a) yields the necessary strength of reinforcement equal to $k_t/\gamma H = 0.0426$, while for the same type of mechanism but with surface BD not being forced to be vertical, $k_t/\gamma H = 0.0501$. The latter is a much better estimate, yet not as good as the one based on the mechanism in Fig. 2(c), $k_t/\gamma H = 0.0570$ (all being lower bounds to the true value of $k_t/\gamma H$).

6. Length of reinforcement

Design of reinforcement entails both its strength and its length. Two failure modes are used in limit analysis of slopes and walls to determine the necessary length of reinforcement: pull-out, and direct sliding over a single reinforcement layer.

Whenever the pull-out force (Eq. (13)) is lower than the reinforcement tensile strength, the pull-out force should be taken in calculations of the rate of work dissipation (Eq. (12)). Since the pull-out force depends on the reinforcement length, the lower bound to the necessary length can be determined from the theorem in Eq. (3). This method is illustrated in the example of the simple mechanism in Fig. 9(a).

With some layers being pulled out during the incipient slope collapse, the equation in (14) takes the form

$$\left(\sum_1^m T_p + (n-m)T_t\right) v\cos(\theta - \varphi) = \frac{\gamma H^2}{2}(\cot\theta - \cot\beta)\, v\sin(\theta - \varphi), \tag{17}$$

where m is the number of reinforcement layers that are being pulled out, and n is the total number of layers. Considering T_p as expressed in Eq. (13), and $T_t = k_t H/n$, and rearranging Eq. (17), one obtains

$$\frac{k_t}{\gamma H} = \frac{n}{n-m}\left[\frac{1}{2}(\cot\theta - \cot\beta)\tan(\theta - \varphi) - \frac{2\mu}{H^2}\sum_{1}^{m} l_{ei} z_i^*\right], \tag{18}$$

where z_i^* is the overburden depth of layer i, and l_{ei} is the effective length of layer i, which, for the mechanism in Fig. 9(a), is

$$l_{ei} = L - (H - z_i)(\cot\theta - \cot\beta), \tag{19}$$

where L is the total length of reinforcement, and z_i is its depth (Fig. 9(a)). Now, given the length of reinforcement L, one can calculate the necessary strength from Eq. (18). If the strength, $k_t/\gamma H$, calculated from Eq. (18), is less than that from Eq. (15), then the reinforcement is longer than necessary. The reinforcement length is sufficient if the strength from Eq. (18) is equal to that from Eq. (15). Increase of the length beyond this length does not improve the safety of the structure.

The necessary length of reinforcement can thus be found from Eq. (18), where the result from Eq. (15) is substituted for the left-hand-side. The maximum of L needs to be found from Eq. (18) with θ being variable. The specific forms of Eqs. (18) and (15) will be different for other failure mechanisms, but the method illustrated can be applied to any mechanism. It needs to be noticed that the length of reinforcement depends on the number of layers and their distribution.

The second criterion for calculation of the length of reinforcement in slopes and walls is the direct sliding of the soil over one layer of reinforcement. Direct sliding is consistent with translational mechanisms, and the one presented in Fig. 10 is

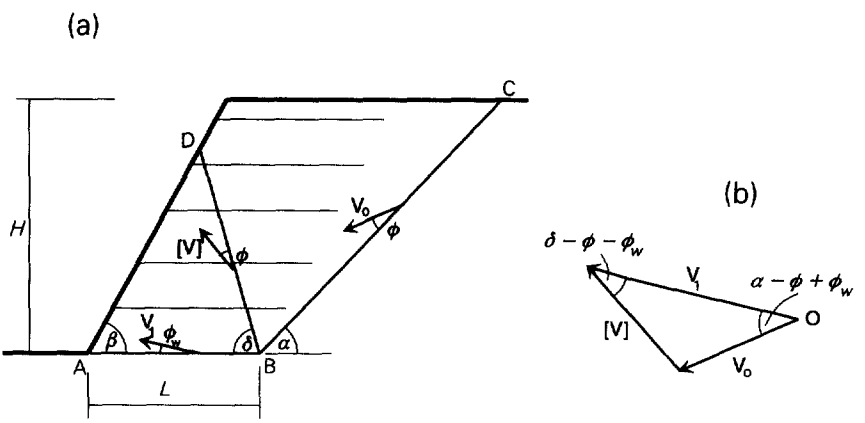

Fig.10. Direct sliding over reinforcement: (a) collapse pattern, and (b) hodograph.

commonly used for slopes and walls. Blocks BCD and ABD move with velocities v_0 and v_1, respectively, and [v] is the velocity jump at interface BD. The associative sliding rule on the reinforcement sheet requires that velocity v_1 be inclined to the reinforcement sheet at soil-reinforcement friction angle φ_w. The soil–geosynthetic friction coefficient for direct sliding is expressed here as fraction f_d of the tangent of the internal friction angle, i.e., $\varphi_w = \tan^{-1}(f_d \tan\varphi)$. Limit analysis leads to the lower bound for the length necessary to prevent direct sliding. This length is calculated from Eq. (3) in which the left hand side is replaced by the work dissipation rate in the reinforcement layers intersecting failure surface *BD*, and the right hand side represents the work rate of the weight of blocks BCD and ABD. Maximum of the length should be sought from such balance (best lower bound), with angles δ and α being variable.

7. Distribution of reinforcement

Calculations using the kinematic approach of limit analysis are based on a work-rate balance equation (Eq. (3)), which can be solved for one unknown only. This unknown may be the lower bound to the necessary strength of reinforcement, or upper bound to a limit load (or a safety factor). The technique does not permit evaluation of the distribution of limit loads, distribution of forces in reinforcement, etc. The same is true for the limit equilibrium technique. Both techniques are based on the premise that both the reinforcement and the soil are in the limit state. Hence, it is assumed that the forces in the reinforcement layers at failure surfaces all reach the reinforcement strength. However, the distribution of the forces along a single reinforcement layer is not determined.

The influence of distribution of reinforcement layers (spacing) on the necessary strength of reinforcement can be addressed using limit state techniques, provided a realistic mechanism is considered in the analysis. An example is shown in Figs. 9(c) and (d) where the same amount of reinforcement is used, but it is distributed differently. The spacing in Fig. 9(d) is varied to match the triangular distribution of the 'smeared' strength. The energy dissipation rate due to reinforcement failure is different in both cases since the velocity discontinuity vector along BC is not uniform (also, the most critical failure surface is not the same in the two cases). The distribution in Fig. 9(d) is more effective, since it yields a larger energy dissipation rate. Consequently, the calculated lower bound to the required reinforcement strength ($k_t/\gamma H = 0.0497$ for $\beta = 60°$ and $\varphi = 35°$) is smaller than that for the uniform reinforcement distribution ($k_t/\gamma H = 0.0570$).

In order to address the issue of the influence of the reinforcement distribution (spacing) on the reinforcement amount/strength, safety factor, etc., the mechanism considered must be sensitive to this distribution. Whereas it was already shown that the distribution of reinforcement affects the energy dissipation rate for the rotational mechanism (Fig. 9(c,d)), the dissipation for translational mechanisms in Fig. 3(a) and Fig. 9(a,b) is independent of the reinforcement distribution. Indeed, these modes are not very realistic.

8. Final remarks

The kinematic approach of limit analysis constitutes a convenient tool for stability analysis of reinforced soil structures. It provides a rigorous bound to the exact solution (lower bound to the strength of reinforcement, or upper bound to the loads causing failure). The method is based on the construction of kinematically admissible collapse mechanisms, and the balance of the work rate in an incipient failure process. A dual formulation of the kinematic limit analysis is possible in terms of the equilibrium of limit forces. However, the kinematics is not made explicitly part of the limit equilibrium method. Therefore, the mechanisms considered in the traditional limit equilibrium analyses are not always kinematically admissible, and they lead to solutions whose accuracy cannot be assessed easily. Limit analysis based on the kinematic approach removes ambiguities that arise in traditional techniques. Limit analysis yields a rigorous bound to an exact solution. Therefore, it is possible to assess which among the admissible solutions is the closest to the exact one (even though the exact solution is not known). Two very important aspects of limit analysis is assuring that the collapse mechanisms considered in stability calculations are kinematically admissible, and that their geometry is varied so as to obtain the best bound to the unknown quantity (amount or strength of reinforcement, or limit load).

Both limit equilibrium and limit analysis were used to address the issue of the inclination of the reinforcement force at a failure surface. Limit analysis indicates that computations should be performed as if the direction of placement of the reinforcement (typically horizontal) was not changed, since its inclination does not influence the result for the tensile failure mode. Only after a more detailed limit force equilibrium analysis does it become clear that the reinforcement force direction should be taken as horizontal.

Limit equilibrium solutions often suffer from assumptions that are not consistent with rigorous limit state analysis (these assumptions affect the accuracy of solutions). The two most common ones are: assuming inclination of interaction forces at rupture surfaces at angles other than φ (to the surface normal), and ignoring the influence of reinforcement at some rupture surfaces. From the limit analysis standpoint such assumptions are kinematically inadmissible. Rupture surfaces cannot occur unless the (Mohr–Coulomb) yield condition is reached, and the mechanism is not admissible unless the reinforcement across any rupture surface fails by tensile collapse or pull-out.

Acknowledgement

The work presented in this paper was sponsored by the National Science Foundation, grant No. CMS-9634193.

References

Anthoine, A., 1989. Mixed modelling of reinforced soils within the framework of the yield design theory. Computers and Geotechnics 7 (1&2) 67–82.

Bathurst, R.J., Alfaro, M.C., 1996. Review of seismic design, analysis and performance of geosynthetic reinforced walls, slopes and embankments. In: International Symposium on Earth Reinforcement, Keynote lecture, Kyushu, pp. 23–52.

Davis, E.H., 1968. Theories of plasticity and the failure of soil masses. In: Soil Mechanics: Selected Topics, I.K. Lee (Ed.), Butterworth, London, pp. 341–380.

de Buhan, P., Mangiavacchi, R., Nova, R., Pellegrini, G., Salençon, J., 1989. Yield design of reinforced earth walls by homogenization method. Géotechnique 39 (2) 189–201.

de Buhan, P., Salençon, J., 1993. A comprehensive stability analysis of soil nailed structures. Eur. J. Mech., A/Solids 12, 325–345.

Drucker, D.C., Prager, W., Greenberg, H.J., 1952. Extended limit design theorems for continuous media. Quart. Appl. Math. 9, 381–389.

Gourc, J.P., Ratel, A., Delmas, Ph., 1986. Design of fabric retaining walls: The Displacement Method. Third International Conference on Geotextiles, Vol II, Vienna, 289–294.

Gvozdev, A.A., 1938. The determination of the value of the collapse load for statically indeterminate systems undergoing plastic deformation (1960 translation from Russian by R.M. Haythornthwaite). Int. J. Mech. Sci. 1 (1960) 322–335.

Hill, R., 1948. A variational principle of maximum plastic work in classical plasticity. Quart. J. Mech. Appl. Math. 1, 18–28.

Holtz, R.D., Christopher, B.R., Berg, R.R., 1997. Geosynthetic Engineering. BiTech Publ., Richmond, BC.

Jewell, R.A., 1990. Revised design charts for steep reinforced slopes. In: Reinforced Embankments, Theory and Practice, Thomas Telford, London, pp. 1–30.

Koerner, R.M., 1998. Design with Geosynthetics. 4th. edition, Prentice Hall, Upper Saddle River.

Leshchinsky, D., Boedecker, R.H., 1989. Geosynthetic reinforced soil structures. J. Geot. Eng. 115 (10) 1459–1478.

Michalowski, R.L., 1997. Stability of uniformly reinforced slopes. J. Geot. Geoenv. Engrg. 123, 546–556.

Michalowski, R.L., Shi, L., 1993. Bearing capacity of nonhomogeneous clay layers under embankments. J. Geot. Engrg. 119 (10) 1657–1669.

Michalowski, R.L., Zhao, A., 1995. Continuum versus structural approach to stability of reinforced soil. J. Geot. Engrg. 121 (2) 152–162.

Michalowski, R.L., Shi, L., 1997. A note on strain localization in punch-indentation laboratory tests of sand. 4th. International Workshop on Localization and Bifurcation Theory for Soils and Rocks, 29 September–2 October, 1997, Gifu, Japan (abstract).

Salençon, J., 1990. An introduction to the yield design theory and its applications to soil mechanics. Eur. J. Mech., Ser. A/Solids 9 (5) 477–500.

Sawicki, A., and Leśniewska, D., 1989. Limit analysis of cohesive slopes reinforced with geotextiles. Computers and Geotechnics 7 (1&2) 53–66.

Shi, L., 1996. Failure loads on layered soils and mechanisms of collapse. Thesis, Johns Hopkins University, Baltimore.

Wright, S.G., Duncan, J.M., 1991. Limit equilibrium stability analyses for reinforced slopes. Transp. Res. Board 1330, 40–46.